Tunnelling spectra of individual magnetic endofullerene molecules

JACOB E. GROSE[1], EUGENIA S. TAM[1], CARSTEN TIMM[2], MICHAEL SCHELOSKE[3], BURAK ULGUT[4], JOSHUA J. PARKS[1], HÉCTOR D. ABRUÑA[4], WOLFGANG HARNEIT[3] AND DANIEL C. RALPH[1]*

[1]Laboratory of Atomic and Solid State Physics, Cornell University, Ithaca, New York 14853, USA
[2]Department of Physics and Astronomy, University of Kansas, Lawrence, Kansas 66045, USA
[3]Institut für Experimentalphysik, Freie Universität Berlin, Arnimallee 14, 14195 Berlin, Germany
[4]Department of Chemistry and Chemical Biology, Cornell University, Ithaca, New York 14853, USA
*e-mail: ralph@ccmr.cornell.edu

Published online: 19 October 2008; doi:10.1038/nmat2300

The manipulation of single magnetic molecules may enable new strategies for high-density information storage and quantum-state control. However, progress in these areas depends on developing techniques for addressing individual molecules and controlling their spin. Here, we report success in making electrical contact to individual magnetic N@C_{60} molecules and measuring spin excitations in their electron tunnelling spectra. We verify that the molecules remain magnetic by observing a transition as a function of magnetic field that changes the spin quantum number and also the existence of non-equilibrium tunnelling originating from low-energy excited states. From the tunnelling spectra, we identify the charge and spin states of the molecule. The measured spectra can be reproduced theoretically by accounting for the exchange interaction between the nitrogen spin and electron(s) on the C_{60} cage.

Magnetic molecules provide the opportunity to study, at a fundamental level, the origins of ferromagnetism and quantum aspects of magnetic dynamics[1,2]. Proposals suggest that their spin degrees of freedom could also serve as useful qubits for quantum manipulation[3]. Most previous experiments on magnetic molecules have examined samples consisting of many molecules; however, applications and more detailed scientific studies will require the ability to address individual molecules. Here, we report the use of tunnelling spectroscopy within single-molecule transistors (SMTs), a technique that has been used previously to measure vibrational and electronic excitations[4–6], to achieve electrical contact to individual molecules of the spin-3/2 endohedral fullerene N@C_{60} (Fig. 1a) and to measure its spin excitations. N@C_{60} is an attractive model system[7,8] because of its simple spin structure and because of the possibility of control experiments using non-magnetic C_{60} molecules[4,9–14]. N@C_{60} molecules also have the advantage of being stable[15] at the high temperatures present during the electromigration process by which our molecular-scale junctions are formed[16,17]. Previous SMT experiments using less robust Mn_{12}-based magnetic molecules detected magnetic signatures in a few samples[18,19], but found that the molecular magnetism was usually destroyed during device fabrication[19]. We observe that the N@C_{60} devices exhibit clear magnetic character, in that they have a spin-state transition as a function of applied magnetic field. The nature of this transition enables us to identify the charge and spin states of the molecule in the SMT. The spectra of N@C_{60} also exhibit low-energy excited states and signatures of non-equilibrium spin excitations predicted for this molecule[20]. We associate the existence of a spin transition in N@C_{60} accessible at laboratory magnetic fields with the scale of the exchange interaction between the nitrogen spin and electron(s) on the C_{60} cage.

The geometry of our SMT devices is shown in Fig. 1b. We make the devices by adsorbing the molecules onto an initially continuous Pt wire on top of an oxidized Al gate electrode and then breaking the wire using electromigration to form a nanometre-scale gap. (Extra information about fabrication procedures is given in the Methods section.) We identify the presence of one or more molecules in the gap by the observation of gate-dependent Coulomb-blockade transport characteristics[5,11]. Our success rate for obtaining such devices was 9/19 for N@C_{60} devices and 17/59 for C_{60} devices, whereas 0/39 control samples prepared using pure toluene instead of a fullerene solution showed Coulomb blockade. Six of the N@C_{60} devices were sufficiently stable for detailed measurements.

The most striking difference between the N@C_{60} devices and the C_{60} controls is seen in the magnetic-field dependence of the tunnelling conductance spectra. Figure 2 shows these spectra as a function of source–drain voltage (V) and magnetic field (B) at dilution-refrigerator temperatures (electron temperature $\approx$100 mK) for values of gate voltage (V_g) slightly more positive than the 'degeneracy point'—the value of gate voltage for which the energy difference between the two accessible charge states is zero, so that current can flow even near $V = 0$. Figure 3 shows the conductance for each sample as a function of V and V_g near the degeneracy point. (By focusing on low-voltage transport near one degeneracy point, we ensure that tunnelling is occurring through a single molecule[5].) In the N@C_{60} devices, as a function of increasing B (Fig. 2a,b), the lowest-voltage conductance peaks at positive and negative bias first move apart and then change slope to move back closer together. These initial peaks can be associated with the same quantum transition from the ground state of one charge state (charge q) of the molecule to the ground state with charge $q+1$ (one fewer electron). At the value of B where the slopes of the

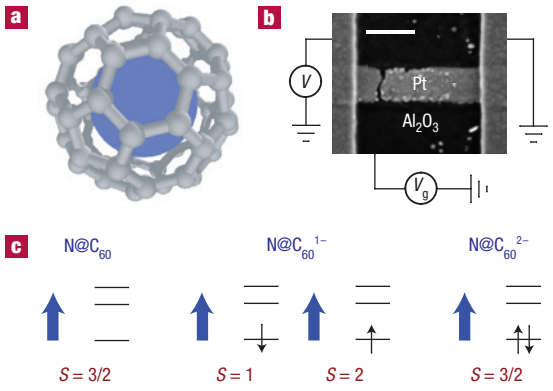

Figure 1 Device geometry and the spin states of N@C_{60}. a, Schematic diagram of the N@C_{60} molecule. **b**, Scanning electron microscopy image of a sample at room temperature following electromigration. The scale bar denotes 200 nm. The circuit schematic diagram shows our biasing convention. **c**, Spin states for N@C_{60} and its anions. The blue arrows represent the $S_N = 3/2$ spin of the N atom. The horizontal black lines represent the lowest unoccupied orbitals of the C_{60} molecule. The possible total spin states of the N@C_{60} ion are indicated.

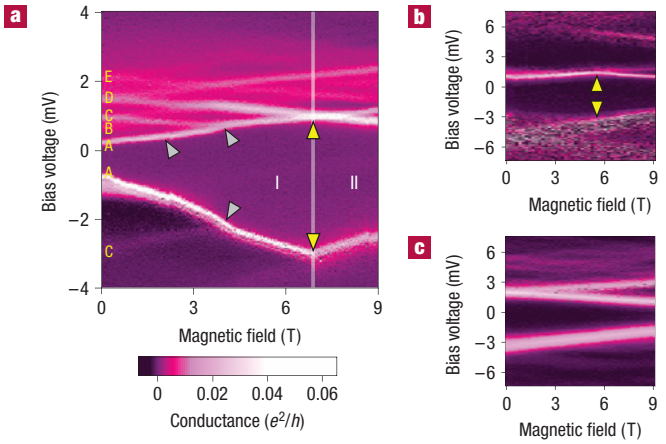

Figure 2 Colour-scale plots of differential conductance (dI/dV) for N@C_{60} and C_{60} SMTs. a, dI/dV for N@C_{60} device 1 as a function of source–drain voltage and applied magnetic field at constant value of gate voltage $V_g = -891$ mV on the positive side of the degeneracy point. Yellow triangles indicate a change in slope of the ground-state peaks, and grey triangles mark the non-crossing levels discussed in the text. The labels designate different transitions. In region I, the ground-state transition corresponds to decreasing spin, $S_{z,q+1} - S_{z,q} < 0$, whereas in region II $S_{z,q+1} - S_{z,q} > 0$. **b**, Same as **a** for N@C_{60} device 2. The maximum of the colour scale is 0.15 e^2/h. **c**, dI/dV as a function of V and B at constant V_g on the positive side of the degeneracy point for a C_{60} SMT. The maximum of the colour scale is 0.02 e^2/h. No change in slope is observed for the ground-state peaks of C_{60}.

peaks change sign in Fig. 2a, we observe level crossings, where a conductance peak that at low B is associated with an excited state of charge $q+1$ becomes the ground state of charge $q+1$ at high B. We measured ground-state conductance peaks that shift apart then together as a function of B on the positive-gate side of the degeneracy point in four out of five of the N@C_{60} devices on which we carried out this measurement. (The fifth showed no change in slope up to 9 T.) The field values at which the crossovers occurred varied from approximately 1 to 7 T.

The level crossing in Fig. 2a shows that the change in sign of the ground-state-peak slopes is due to an increase in total spin component $S_{z,q+1}$ along the magnetic-field direction $\hat{z}$ for the lowest-energy charge $q+1$ state. The slopes of the peaks as a function of B imply that at low fields $S_{z,q} > S_{z,q+1}$ and at high fields $S_{z,q} < S_{z,q+1}$. Assuming that $|S_{z,q+1} - S_{z,q}| = 1/2$, the slopes of the conductance resonances versus magnetic field shown in Fig. 2 correspond to an electronic g-factor $|g| = 2.0 \pm 0.3$.

In contrast, Fig. 2c shows the tunnelling spectrum for a C_{60} device also taken on the positive-gate side of its degeneracy point. Of the five C_{60} devices we measured as a function of magnetic field, none showed a change in the sign of the slopes for the lowest-voltage tunnelling transition. Although the spectra for the C_{60} devices often contain low-energy excitations in the same range of energy as those of N@C_{60}, 0.1 meV to several millielectronvolts, the lack of spin transitions suggests that the low-lying excitations in C_{60} are vibrational satellites[4,11,21], rather than being electronic or magnetic states.

Recently, a tunnelling transition with a change in slope as a function of magnetic field has been observed in a C_{60} device, for gate voltages in a limited range near the middle of one Coulomb-blockade region[14]. Our measurements showing no such level crossing in C_{60} devices are not in conflict with ref. 14 because our data for C_{60} and N@C_{60} probably correspond to a different charge state, and our measurements were made only for gate voltages near the degeneracy point, well away from the middle of any Coulomb-blockade region.

We assert that the spin-state transition in the N@C_{60} devices is probably associated with two states with different values of total spin, as opposed to two states within the same multiplet split by magnetic anisotropy. Because any magnetic anisotropy axes could be oriented arbitrarily relative to the applied magnetic field, if the transition were due to states split by magnetic anisotropy it should be expected, in general, that the slopes of the energy levels as a function of B should show deviations from $|g| = 2$ and exhibit strong deviations from linearity at low field[19,22,23]. In our data, the field dependence of the transitions is very close to linear (away from localized kinks associated with level crossings). The lack of observable magnetic anisotropy effects is consistent with the symmetries of N@C_{60} and the weak spin–orbit coupling of its constituent atoms[24].

With this understanding, the existence of a spin-state transition at an accessible magnetic field for the charge $q+1$ energy levels of N@C_{60} enables us to identify the charge and spin states involved in the tunnelling. Consider the possible states shown in Fig. 1c, which depicts the nitrogen spin (blue arrow) coupled to electron spins (black arrows) occupying the lowest unoccupied molecular orbital (LUMO) of the C_{60} molecule. We assume that a three-fold degeneracy of the LUMOs of isolated C_{60} is broken by molecular deformation due to interaction with the electrodes or the Jahn–Teller effect[25], and we consider only the experimentally accessible neutral and negative charge states. Neutral N@C_{60} is known to have spin 3/2 because the encapsulated nitrogen retains its atomic electronic configuration[26]. When electrons are added to N@C_{60}, they are believed to occupy the LUMO of the C_{60} molecule[27]. With the addition of one extra electron, N@C_{60}^{1-} may therefore have either $S = 1$ or 2, and these two multiplets are split in energy by the exchange interaction between the N spin and the electron spin. If the exchange is antiferromagnetic, the ground state will have $S = 1$ for low B and $S = 2$ for large B. For N@C_{60}^{2-}, the total spin should again be $S = 3/2$ because the splitting between the LUMO states is expected to be large compared with Hund's rule coupling. Because we observe the

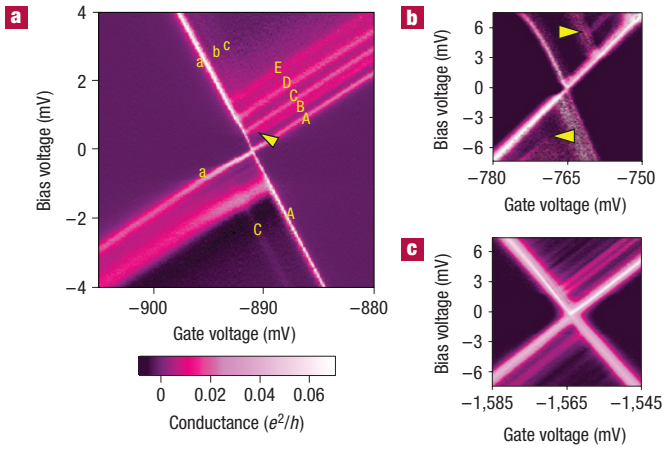

Figure 3 Colour-scale plots of differential conductance (dI/dV) as a function of bias voltage and gate voltage at zero applied field ($B = 0$ T). a,b, dI/dV from the same N@C_{60} devices, 1 and 2, shown in Fig. 2a and b, respectively. The labels in **a** designate different transitions, consistent with Fig. 2a. Their energies, determined by extrapolating the transition lines to the Coulomb-blockade threshold, are (± 0.02 meV) $E_B - E_A = 0.29$ meV, $E_C - E_A = 0.48$ meV, $E_D - E_A = 0.93$ meV, $E_E - E_A = 1.35$ meV, $E_b - E_a = 0.20$ meV and $E_c - E_a = 0.41$ meV. The triangles indicate the termination of ETE peaks associated with non-equilibrium excitations. **c**, dI/dV for the same C_{60} device shown in Fig. 2c. No ETE peaks are visible for this non-magnetic molecule.

spin-state transition in the more positive of the two charge states involved in tunnelling, the 0/1− charge couple can be ruled out as the charge states between which tunnelling occurs. This leads to the identification, for an antiferromagnetic exchange interaction, that 1−/2− is the couple with the lowest charge magnitude that is capable of transitioning from $S_q - S_{q+1} = +1/2$ at low fields to $S_q - S_{q+1} = -1/2$ at high fields. For a ferromagnetic exchange interaction, the lowest-magnitude charge couple possibly consistent with the data would be 2−/3−, which is unlikely because the 3− charge state should have a much higher energy than 1− or 2− states. A 2−/3− scenario would also require fine tuning such that the exchange splitting is approximately equal to the deformation-induced level splitting within the N@C_{60}^{2-} LUMO.

The identification of our measured spectra with the 1−/2− charge couple implies that our N@C_{60} devices are in the 2− charge state at $V_g = 0$, which may seem to be a large magnitude of charge in an unbiased device. However, for C_{60} in the gas phase, both the 1− and 2− states are more stable than the neutral form, with the 2− state quite close in energy to the 1− state[28–30]. The equilibrium charge of C_{60} is generally found to be either 1− or 2− when it is adsorbed on noble metal surfaces[31,32]. These previous studies suggest that the 3− charge state is likely to have a much higher energy than 1− or 2− in an unbiased device, which argues against the possibility of a ferromagnetic exchange interaction in our samples as this would require a 2−/3− charge couple with a 3− charge state at zero gate voltage. In regard to the sign of the exchange interaction, an *ab initio* calculation has predicted a weakly ferromagnetic interaction in N@C_{60}^{1-}, rather than the antiferromagnetic interaction we suggest[33]. However, it should be noted that the calculation of the exchange interaction is difficult because it is computed as a small difference between large total energies.

The device-to-device variations that we measure in the N@C_{60} tunnelling spectra indicate that the energies of the electronic states are perturbed differently by the environment in each device. To explain the variations in field value giving rise to the spin-state transition, the strength of the exchange interaction must differ between devices, presumably owing to different amounts of molecular deformation and/or local electric fields. If we parameterize the exchange interaction in the form $J\mathbf{s}_e \cdot \mathbf{S}_N$, where $\mathbf{s}_e$ is the total electron spin and $\mathbf{S}_N$ is the spin on the nitrogen atom, then measured transition fields (1–7 T) imply exchange strengths, $|J|$, between 0.06 and 0.4 meV.

To understand how the measured tunnelling spectra might relate to the molecular magnetism, we have calculated the conductance of a N@C_{60} transistor (Fig. 4a,b). As a minimal model to account for the low-energy transitions, we consider the energy level diagrams shown in Fig. 4c,d, which include the three multiplets, ($q = -2$, $S = 3/2$), ($q = -1$, $S = 1$) and ($q = -1$, $S = 2$), we have introduced previously and also the lowest-energy excited-state multiplet associated with each of these states. The excited multiplets could correspond to the added excitation of a long-lived vibrational mode or energy shifts due to charging in nearby molecules. We assume that the molecule has negligible magnetic anisotropy, so that all of the magnetic effects we consider are due to exchange-induced level splittings. This is in contrast to previous calculations for Mn_{12}-type molecules where the low-energy spectra were assumed to be dominated by large magnetic anisotropy[18,19]. We use the rate-equation approach to calculate the differential conductance. Parameter values, listed in the Methods section, are selected to approximate the data in Figs 2a and 3a.

There are a sufficiently large number of free parameters that we do not seek or claim quantitative agreement. Depending on assumptions about the value of J and vibrational parameters, different numbers of excited-state tunnelling transitions are possible. Nevertheless the calculation can reproduce many of the qualitative features seen in Figs 2 and 3. First, the N@C_{60} spectra shown in Fig. 3a,b and the theoretical results shown in Fig. 4b both exhibit a pattern of non-equilibrium excitations that was predicted[20] for spin excitations in N@C_{60}. If the conductance peaks marked by yellow triangles in Fig. 3a,b are extrapolated towards zero voltage, they do not extend all the way to the line corresponding to the ground-state tunnelling threshold, but instead terminate when they intersect a conductance peak corresponding to an excited-state transition. We observed this type of feature in four of six N@C_{60} devices, but in none of thirteen C_{60} devices that were stable enough for detailed study (for example, see Fig. 3c). This type of phenomenon, which has been measured previously in metal and semiconductor quantum dots[34,35], can be understood[20] in terms of excited-state to excited-state (ETE) transitions within the spectrum of energy levels in N@C_{60}. The idea is illustrated by Fig. 4c,d. Here, ground-state tunnelling at low magnetic field corresponds to the transition (labelled A) from the $q = -2$, $S = 3/2$ state to $q = -1$, $S = 1$. For a sufficiently large applied voltage V, the tunnelling of an electron back into the molecule can lead to a transition (labelled b) from the $q = -1$, $S = 1$ state to the excited $q = -2$, $S = 3/2$ multiplet, rather than the ground-state $S = 3/2$ multiplet. If this excited state does not relax before the next electron tunnels out of the molecule, this will produce an ETE conductance peak corresponding to a transition (B) between the excited $q = -2$, $S = 3/2$ multiplet and the excited $q = -1$, $S = 2$ multiplet. The reason that transition B cannot extrapolate indefinitely to lower voltage is that the applied bias must provide sufficient energy to permit the transition b for transition B to be possible. As support for this interpretation, note that the level diagram in Fig. 4c,d requires that $E_C = E_B + (E_b - E_a)$. Using the measured values of the excitation energies (see the caption for Fig. 3), this equality is satisfied within experimental uncertainty.

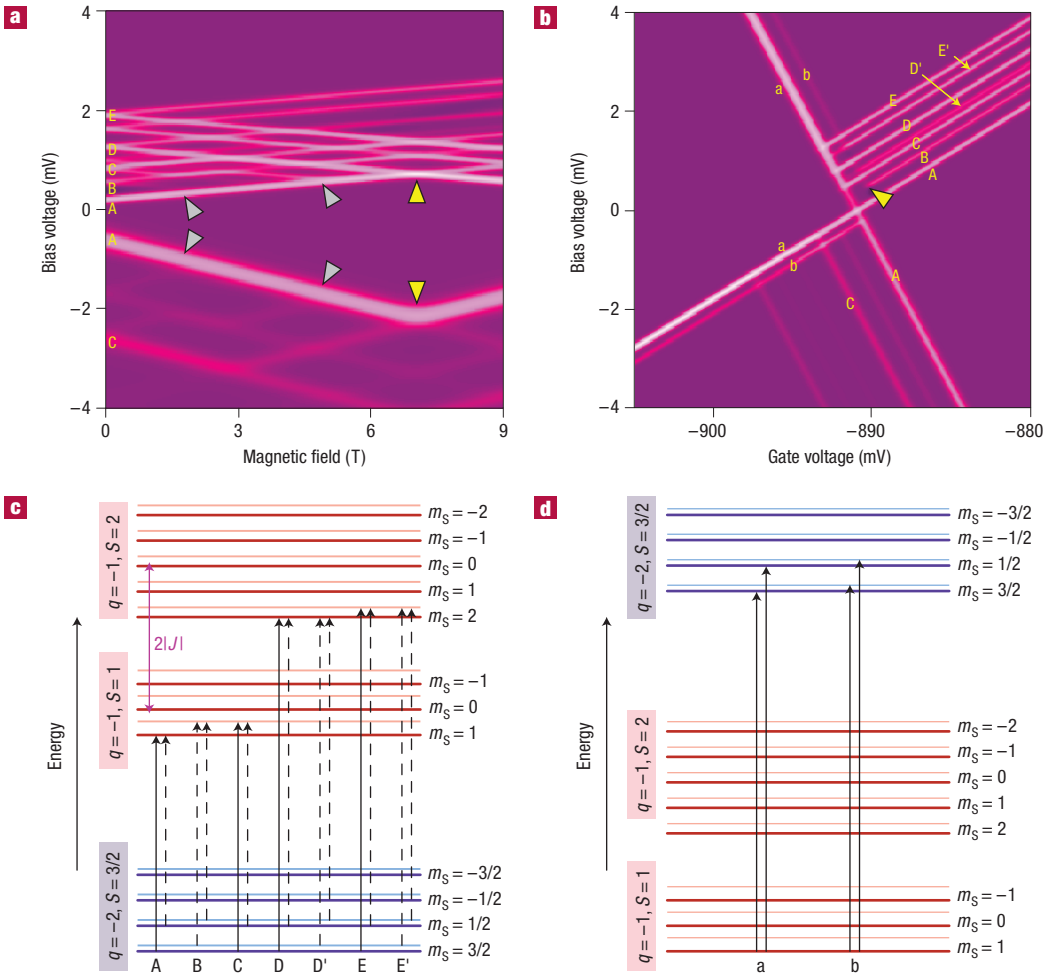

Figure 4 Numerical calculation of the tunnelling spectrum for N@C_{60}, with parameters chosen to mimic the data for device 1. a, Calculated dI/dV as a function of V and B at constant V_g on the positive side of the $q=-2/q=-1$ degeneracy point. Compare with Fig. 2a. The yellow triangles mark the spin-state transition and the grey triangles mark non-crossing levels. **b**, Calculated dI/dV as a function of V and V_g. The triangle marks the termination of a non-equilibrium ETE peak. Compare with Fig. 3a. **c**, Energy level diagram for a large applied magnetic field showing allowed tunnelling transitions that contribute to the low-energy spectrum, for tunnelling from the charge $q=-2$ states (blue) to the $q=-1$ states (red) of N@C_{60}. The dashed lines show non-equilibrium transitions. (For $B=0$, the different m_S levels within a given multiplet will become degenerate in the absence of magnetic anisotropy.) **d**, Allowed tunnelling transitions contributing to the low-energy spectrum, for tunnelling from $q=-1$ states to $q=-2$ states. The letters labelling the transitions in **c** and **d** can explain the labelled states in Figs 2a and 3a. The relative energies of the $q=-1$ and -2 states will depend on V_g.

Another successful feature of the calculation is that it can account for the magnetic-field dependence of the tunnelling spectrum shown in Fig. 2a. In particular, note that this spectrum has two conductance peaks that as a function of magnetic field intersect the lowest-voltage transition but then terminate so that they do not produce a level crossing—this happens near 1.5 T for transition B and 4 T for transition C. Only near 7 T is there a true level crossing for transition D that corresponds to the spin-state transition discussed above. The 'non-crossing' levels can be understood as another consequence of non-equilibrium ETE transitions. For voltages less than the ground-state to ground-state transition, the first electron tunnelling event that initiates current flow is not allowed, so that the excited states cannot be populated.

One difference between the calculated spectrum in Fig. 4a,b and the measurements in Figs 2a and 3a is that the calculated spectrum contains two more lines at positive bias (seven lines at $B=0$ instead of five). The extra lines (D′ and E′) correspond to non-equilibrium ETE transitions from the excited $q=-2$, $S=3/2$ state to the two $q=-1$, $S=2$ states (that is, they are lower-energy satellites of transitions D and E.) We suspect that these extra transitions are present but unresolved in the experimental spectra because the linewidths of the experimental transitions increase as a function of energy and the ETE transitions have weaker amplitudes than transitions originating from the ground state, thereby making them difficult to distinguish at higher energies. The level broadening with increasing energy is not included in our simple model, but if we add in the measured broadening by hand, the transition D′ is completely obscured and E′ becomes only marginally resolvable.

The capability to make electrical contact to single magnetic molecules without destroying their magnetic character provides the foundation for more advanced strategies to manipulate spin states. We have shown that the charge and spin values of the molecule can be identified, that spin excitation energies can be measured and that the tunnelling spectrum of N@C_{60} can be

understood qualitatively within an elementary model. The next challenges will include developing the means to coherently populate desired superpositions of spin states (using, for instance, applied microwaves[3,36]), developing accurate techniques to read out spin information and achieving improved control over the interaction between the magnetic molecule and its environment so as to minimize device-to-device variations.

METHODS

SYNTHESIS

$N@C_{60}$ was synthesized by continuous nitrogen ion implantation into freshly sublimed fullerene layers[26] with a yield ($N@C_{60}$:C_{60} ratio) of $\sim 10^{-4}$. The $N@C_{60}$ contained in the harvested product was enriched and purified by multi-step high-pressure liquid chromatography[37]. Purity was checked by ultraviolet–visible absorption, high-pressure liquid chromatography and electron spin resonance and found to be better than 99.5%.

ELECTROCHEMISTRY

We have confirmed, using electrochemical measurements, that the interaction in $N@C_{60}$ between the N atom and the extra electrons on C_{60} is relatively weak. Cyclic voltammograms were carried out on $N@C_{60}$ or C_{60} films formed by drop-casting from toluene solutions onto a 3 mm Pt disc electrode, polished to a mirror finish, used as the working electrode. A Ag/AgCl (saturated NaCl) and a Pt coil were used as the reference and counter electrodes, respectively. The scans, carried out at a sweep rate of 500 mV s^{-1}, were done in 0.1 M tetrabutylammonium hexafluorophosphate in acetonitrile in a single-compartment cell. The solution was deoxygenated by N_2 bubbling for 10 min before the sweeps, which were run in a N_2 atmosphere. We found that the first two reductions of $N@C_{60}$ occur within 25 mV of those of C_{60}. The $\sim$25 mV shifts are not related to the nature of the molecules and can be attributed to the varying rates of dissolution of the reduced species due to slight variations in the film morphology. This arises as a result of the fact that whereas the neutral forms of C_{60} and $N@C_{60}$ are insoluble in acetonitrile, the reduced forms are not.

SAMPLE FABRICATION

Our SMTs were fabricated following a procedure similar to those used previously[4,5]. First, we made an Al gate electrode 16 nm thick and 2 μm wide on an oxidized Si wafer, and exposed the Al to air to form a thin insulating oxide. On top of the gate electrode, we fabricated continuous Pt wires with widths of approximately 150 nm and thicknesses of 10 nm. The chips were cleaned with an oxygen plasma and immediately covered with 25 μl of either a 0.1 mM solution of $N@C_{60}$ for 2.5 min or (for one type of control sample) a 0.5 mM solution of C_{60} in toluene for 1 min. Then the excess solution was blown off the chip, and the deposition process was repeated. We found that repeating the deposition process produced a more convenient yield of single-molecule devices. After the molecules were deposited, we cooled the devices to cryogenic temperatures and broke the wires using electromigration in a circuit with small series resistance[17], thereby forming nanometre-scale gaps in which a molecule was sometimes trapped. The breaking voltages for our Pt wires were in the range 1–1.5 V.

LOW-TEMPERATURE MEASUREMENTS

The measurements were carried out in a dilution refrigerator equipped with room-temperature low-pass filters and low-temperature copper powder filters on all electrical lines. The electron temperature calibrated on quantum dot samples is <100 mK. The d.c. current was measured as a function of swept source–drain voltage at fixed gate voltage and magnetic field (without a lock-in amplifier), and then the value of the gate voltage or magnetic field was stepped. The differential conductance was calculated by numerical differentiation.

THEORY

The differential conductance dI/dV is calculated using the rate-equation approach in the sequential-tunnelling approximation[20]. The electronic molecular Hamiltonian reads

$$H_{\mathrm{el}} = \left(\varepsilon - eV_{\mathrm{g}}^{*}\right)\sum_{\sigma} a_{\sigma}^{+}a_{\sigma} + U a_{\uparrow}^{+}a_{\uparrow}a_{\downarrow}^{+}a_{\downarrow} - J\,\mathbf{s}_{\mathrm{e}}\cdot\mathbf{S}_{\mathrm{N}} - B\left(s_{\mathrm{e}}^{z} + S_{\mathrm{N}}^{z}\right),$$

where ε is the on-site energy of electrons with spin $\sigma = \uparrow, \downarrow$ created by a_{σ}^{+}, V_{g}^{*} is the electric potential at the position of the molecule, U is the Coulomb repulsion, J is the exchange interaction between the nitrogen spin $\mathbf{S}_{\mathrm{N}}$ and the spin $\mathbf{s}_{\mathrm{e}} = \sum_{\sigma\sigma'} a_{\sigma}^{+}(\boldsymbol{\sigma}_{\sigma\sigma'}/2)a_{\sigma'}$ of the electrons in the LUMO and B is the magnetic field with a factor $g\mu_{\mathrm{B}}$ absorbed. Only one LUMO is included, the other two are assumed to be split off owing to molecular deformation and to not affect dI/dV. The asymmetric contact capacitances and the fact that the bias voltage is applied to the (arbitrarily labelled) left electrode are incorporated by writing $V_{\mathrm{g}}^{*} = \alpha V_{\mathrm{g}} + \beta_{\mathrm{L}} V$ with the applied gate voltage V_{g} and bias voltage V, where $\alpha = 0.15$ and $\beta_{\mathrm{L}} = 0.25$ give the best fit. Asymmetric tunnelling amplitudes $t_{\mathrm{L,R}}$ between the LUMO and the left and right electrodes are assumed; a ratio $t_{\mathrm{L}}/t_{\mathrm{R}} = 0.4$ is used. In addition, we include low-energy excitations of energy $\hbar\omega_n$ in the $n-$ charge state, which in this description for the sake of definiteness we assume to be vibrational. The transition rates between vibrational states contain Franck–Condon matrix elements[38] $M_{nm,n'm'}$ (with electron numbers n, n' and oscillator quantum numbers m, m') with relative values of the non-vanishing components $M_{20,10} = M_{20,11} = M_{21,11} = M_{22,10} = 1$ and $M_{21,10} = 0.7$; the matrix is symmetric. The other parameters used in the calculations are $\varepsilon = -3.23415$, $U = 3.1$, $J = -0.0004$, $k_{\mathrm{B}}T = 0.00002$ all in electronvolts.

Received 12 May 2008; accepted 19 September 2008; published 19 October 2008.

References

1. Gatteschi, D. & Sessoli, R. Quantum tunneling of magnetization and related phenomena in molecular materials. *Angew. Chem. Int. Ed.* **42**, 268–297 (2003).
2. Bogani, L. & Wernsdorfer, W. Molecular spintronics using single-molecule magnets. *Nature Mater.* **7**, 179–186 (2008).
3. Leuenberger, M. N. & Loss, D. Quantum computing in molecular magnets. *Nature* **410**, 789–793 (2001).
4. Park, H. *et al.* Nanomechanical oscillations in a single-C_{60} transistor. *Nature* **407**, 57–60 (2000).
5. Park, J. *et al.* Coulomb blockade and the Kondo effect in single-atom transistors. *Nature* **417**, 722–725 (2002).
6. Liang, W. J., Shores, M. P., Bockrath, M., Long, J. R. & Park, H. Kondo resonance in a single-molecule transistor. *Nature* **417**, 725–729 (2002).
7. Harneit, W. Fullerene-based electron-spin quantum computer. *Phys. Rev. A* **65**, 032322 (2002).
8. Morton, J. J. L. *et al.* Bang-bang control of fullerene qubits using ultrafast phase gates. *Nature Phys.* **2**, 40–43 (2006).
9. Joachim, C. & Gimzewski, J. K. An electromechanical amplifier using a single molecule. *Chem. Phys. Lett.* **265**, 353–357 (1997).
10. Lu, X. H., Grobis, M., Khoo, K. H., Louie, S. G. & Crommie, M. F. Spatially mapping the spectral density of a single C_{60} molecule. *Phys. Rev. Lett.* **90**, 096802 (2003).
11. Yu, L. H. & Natelson, D. The Kondo effect in C_{60} single-molecule transistors. *Nano Lett.* **4**, 79–83 (2004).
12. Pasupathy, A. N. *et al.* The Kondo effect in the presence of ferromagnetism. *Science* **306**, 86–89 (2004).
13. Champagne, A. R., Pasupathy, A. N. & Ralph, D. C. Mechanically-adjustable and electrically-gated single-molecule transistors. *Nano Lett.* **5**, 305–308 (2005).
14. Roch, N., Florens, S., Bouchiat, V., Wernsdorfer, W. & Balestro, F. Quantum phase transition in single-molecule quantum dot. *Nature* **453**, 633–637 (2008).
15. Waiblinger, M. *et al.* Thermal stability of the endohedral fullerenes $N@C_{60}$, $N@C_{70}$, and $P@C_{60}$. *Phys. Rev. B* **64**, 159901(E) (2001).
16. Trouwborst, M. L., van der Molen, S. J. & van Wees, B. J. The role of Joule heating in the formation of nanogaps by electromigration. *J. Appl. Phys.* **99**, 114316 (2006).
17. Taychatanapat, T., Bolotin, K. I., Kuemmeth, F. & Ralph, D. C. Imaging electromigration during the formation of break junctions. *Nano Lett.* **7**, 652–656 (2007).
18. Heersche, H. B. *et al.* Electron transport through single Mn_{12} molecular magnets. *Phys. Rev. Lett.* **96**, 206801 (2006).
19. Jo, M.-H. *et al.* Signatures of molecular magnetism in single-molecule transport spectroscopy. *Nano Lett.* **6**, 2014–2020 (2006).
20. Elste, F. & Timm, C. Theory for transport through a single magnetic molecule: Endohedral $N@C_{60}$. *Phys. Rev. B* **71**, 155403 (2005).
21. Pasupathy, A. N. *et al.* Vibration-assisted electron tunneling in C_{140} single-molecule transistors. *Nano Lett.* **5**, 203–207 (2005).
22. Guéron, S., Deshmukh, M. M., Myers, E. B. & Ralph, D. C. Tunneling via individual electronic states in ferromagnetic nanoparticles. *Phys. Rev. Lett.* **83**, 4148–4151 (1999).
23. Timm, C. Tunneling through magnetic molecules with arbitrary angle between easy axis and magnetic field. *Phys. Rev. B* **76**, 014421 (2007).
24. Huertas-Hernando, D., Guinea, F. & Brataas, A. Spin–orbit coupling in curved graphene, fullerenes, nanotubes, and nanotube caps. *Phys. Rev. B* **74**, 155426 (2006).
25. Green, W. H. *et al.* Electronic structures and geometries of C_{60} anions via density functional calculations. *J. Phys. Chem.* **100**, 14892–14898 (1996).
26. Almeida Murphy, T. *et al.* Observation of atomlike nitrogen in nitrogen-implanted solid C_{60}. *Phys. Rev. Lett.* **77**, 1075–1078 (1996).
27. Pietzak, B., Weidinger, A., Dinse, K.-P. & Hirsch, A. in *Endofullerenes: A New Family of Carbon Clusters* (eds Akasaka, T. & Nagase, S.) 13–65 (Kluwer, 2002).
28. Yang, S. H., Pettiette, C. L., Conceicao, J., Cheshnovsky, O. & Smalley, R. E. UPS of buckminsterfullerene and other large clusters of carbon. *Chem. Phys. Lett.* **139**, 233–238 (1987).
29. Pederson, M. R. & Quong, A. A. Polarizabilities, charge states, and vibrational modes of isolated fullerene molecules. *Phys. Rev. B* **46**, 13584–13591 (1992).
30. Yannouleas, C. & Landman, U. Stabilized-jellium description of neutral and multiply charged fullerenes $C_{60}^{\pm}$. *Chem. Phys. Lett.* **217**, 175–185 (1994).
31. Modesti, S., Cerasari, S. & Rudolf, P. Determination of charge states of C_{60} adsorbed on metal surfaces. *Phys. Rev. Lett.* **71**, 2469–2472 (1993).
32. Swami, N., He, H. & Koel, B. E. Polymerization and decomposition of C_{60} on Pt(111) surfaces. *Phys. Rev. B* **59**, 8283–8291 (1999).
33. Udvardi, L. in *Electronic Properties of Novel Materials—Molecular Nanostructures* (eds Kuzmany, H., Fink, J., Mehring, M. & Roth, S.) 187–190 (AIP, 2000).
34. Deshmukh, M. M. *et al.* Magnetic anisotropy variations and nonequilibrium tunneling in a cobalt nanoparticle. *Phys. Rev. Lett.* **87**, 226801 (2001).

35. Fujisawa, T., Austing, D. G., Tokura, Y., Hirayama, Y. & Tarucha, S. Nonequilibrium transport through a vertical quantum dot in the absence of spin-flip energy relaxation. *Phys. Rev. Lett.* **88**, 236802 (2002).
36. Harneit, W. *et al*. Room temperature electrical detection of spin coherence in C_{60}. *Phys. Rev. Lett.* **98**, 216601 (2007).
37. Jakes, P., Dinse, K.-P., Meyer, C., Harneit, W. & Weidinger, A. Purification and optical spectroscopy of $N@C_{60}$. *Phys. Chem. Chem. Phys.* **5**, 4080–4083 (2003).
38. Koch, J., von Oppen, F., Oreg, Y. & Sela, E. Thermopower of single-molecule devices. *Phys. Rev. B* **70**, 195107 (2004).

Acknowledgements

We thank R. Döring and O. Baßler for their work to synthesize and purify the $N@C_{60}$ and G. R. Hutchison for help with calculations. The research at Cornell was supported by the US NSF (DMR-0520404, DMR-0605742, EEC-0646547, CHE-0403806 and through use of the Cornell Nanofabrication Facility/NNIN). Work in Berlin was supported by the *Bundesministerium für Bildung und Forschung* under contract no. 03N8709.

Author contributions

J.E.G. had the primary role in fabricating the samples, carrying out the measurements and analysing the data, with assistance from E.S.T. and J.J.P. and advice from D.C.R. C.T. carried out the model calculations. M.S. and W.H. led the molecular synthesis, purification and characterization. B.U. and H.D.A. carried out electrochemical characterization. All of the authors contributed to the data analysis and the preparation of the manuscript.

Author information

Reprints and permissions information is available online at http://npg.nature.com/reprintsandpermissions.
Correspondence and requests for materials should be addressed to D.C.R.